Thermoelectric generator under identical temperature-difference conditions

Thanadhol Sukhabot[1], *Prayut* Jiamrittiwong[1,2*], and *Nutdechatorn* Puangngernmak[1]

[1]Department of Energy Technology and Management, Faculty of Science, Energy and Environment, King Mongkut's University of Technology North Bangkok (Rayong Campus), Rayong, Thailand
[2]Research and Development Center for Chemical Engineering Unit Operation and Catalyst Design (RCC), STRI Building, Floor 1st and 7th (Room 702), King Mongkut's University of Technology North Bangkok, Bangkok, Thailand

Abstract Thermoelectric generator (TEG) can directly convert thermal energy to electrical energy using the Seebeck effect. The voltage output of a TEG is a direct variation to the temperature difference between its hot and cold sides, but the impact of temperature distribution on power output is not fully understood. This study evaluated the effect of TEG power output under identical temperature-difference conditions, focusing on the hot and cold side effects. TEG systems with different heating and cooling source temperatures are operated under identical temperature-differences. The system with a higher temperature gradient at the hot side HTR exhibits better performance than the system with a lower temperature gradient at the hot side LTR. The results show that the power output, voltage output, and current output of both conditions differ by 5.85%, 2.71%, and 3.15%, respectively. This difference is attributed to reduced charge carrier mobility due to temperature gradients between the hot and cold sides. The HTR condition promotable for operating a thermoelectric power generator system, the system is turned on frequently.

1 Introduction

Global energy consumption is on the rise, primarily driven by combustion processes. Due to the inherent limitations of combustion efficiency, a significant amount of waste heat is inevitably released into the environment. Waste heat can be categorized into three temperature ranges: high-temperature heat (>300 °C), medium-temperature heat (100-300 °C), and low-temperature heat (<100 °C). High-temperature waste heat, despite being the most readily utilized form, accounts for only 7% of industrial waste heat recovery. On the other hand, medium- and low-temperature waste heat constitute a significant portion of industrial waste heat, yet their utilization remains low at 89% [1]. High-temperature waste heat is often directly employed in conjunction with heat exchangers to transfer thermal energy to other processes or applications [2]. Low-temperature waste heat, while currently underutilized, holds promise for direct conversion into electricity through the use of thermoelectric materials. Commercially available thermoelectric materials are assembled into thermoelectric modules (TEMs), the composition of which adheres to the following [3]. TEMs comprise two key components: n-type and p-type thermoelectric materials. n-type materials have many electrons, the carriers of negative charges, while p-type materials have many holes, the carriers of positive charges. These two materials are strategically interconnected through metal-semiconductor junctions, forming electrically series but thermally parallel arrangements. TEMs can directly generate electricity from heat. When employed as electricity generation systems, TEMs are referred to as thermoelectric generators (TEG). Fig. 1 illustrates the electricity generation mechanism of TEG. Thermoelectric generators operate based on the Seebeck effect, which describes the voltage generated by a temperature difference across a material [4].

$$V = S\Delta T \tag{1}$$

Where

V = Open-circuit voltage (V)
S = Seebeck coefficient (μV/K)
ΔT = Temperature difference (K)

For thermoelectric materials to effectively conduct electricity, they require a temperature gradient, with heat on one side and cooling on the other. This temperature difference drives the movement of electrons, generating an electric current within the circuit. The performance of thermoelectric materials is evaluated using a dimensionless figure of merit known as the ZT value. Ideal thermoelectric materials exhibit a high Seebeck coefficient, high electrical conductivity and low thermal conductivity. The relationship between these parameters is expressed in equation (2):

* Corresponding author: prayut.j@sciee.kmutnb.ac.th

$$ZT = \frac{S^2 \sigma}{k} T \quad (2)$$

Where

ZT = Dimensionless figure of merit
S = Seebeck coefficient (μV/°C)
σ = Electrical conductivity (S/m)
k = Thermal conductivity (W/m·K)

In a closed-circuit system, the internal resistance (R_{int}) also plays a crucial role in the governing equations [5, 6]. The direct proportionality between R_{int} and ΔT significantly impacts the design and optimization of TEG systems. When TEG is employed to recover waste heat from industrial processes, increasing the temperature gradient may be desirable to augment power generation. However, it is essential to acknowledge that this increase also elevates the internal resistance of the TEG, potentially limiting the achievable power output [7]. TEMs typically utilize bismuth telluride (Bi_2Te_3), a promising thermoelectric material for low-temperature applications, particularly around room temperature. Its narrow energy gap and ability to effectively conduct both electrons and holes make it suitable for both n-type and p-type materials. However, its high thermal conductivity compromises its efficiency at elevated temperatures, leading to reduced power generation [8]. TEMs are inherently limited by their low internal efficiency. To enhance their effectiveness, researchers have explored strategies to improve the efficiency of TEMs. One promising approach involves filling the module with insulating material. Studies have demonstrated that filling TEMs with aerogel can lead to an efficiency increase of 8.22%, while ideal insulating materials have the potential to boost efficiency by 9.12% [9]. The impact of the substrate on the performance of both CTEMs (commercial thermoelectric modules) and FTEMs (flexible thermoelectric modules) was investigated, demonstrating the suitability of two distinct substrate applications [10]. The geometric characteristics of thermoelectric legs were investigated, with five leg configurations selected within the module for performance analysis. Utilizing numerical modeling and temperature-dependent properties for Bi_2Te_3, the impact on internal resistance, conductivity, temperature, thermal stress, deformation, and other output parameters was revealed. The X-leg geometry exhibited significant temperature-dependent behavior, and among the five configurations, the highest density proved to be the most efficient [11]. By incorporating nanomaterials, the ZT value of thermoelectric materials can be enhanced, leading to improved efficiency due to reduced thermal resistance [12, 13]. As previously discussed, the focus has been on enhancing efficiency within the TEM itself. However, to improve the overall efficiency of TEG systems currently employed in various applications, such as health monitoring and tracking systems, micro-self-powered wireless platforms, industrial electronic devices, automobile engines, and aerospace, the automotive sector must take a leading role in TEG market development, similar to the research and development (R&D) efforts in thin-film TEG [14]. Enhancing the output power of TEG systems necessitates careful consideration of various factors within the system. A study comparing forced convection heat transfer using fins immersed in cold water and natural convection heat transfer with air revealed that cold water was more effective in stabilizing the cold side temperature, thereby improving TEG performance [15]. The study investigated the effectiveness of non-conductive thermal interface materials (TIMs) in reducing thermal contact resistance within medium-temperature TEG modules. By employing BN paste and polyurethane sheet under a pressure of 1.0 MPa, the study demonstrated the ability of these TIMs to effectively stabilize and enhance the performance of TEGs operating in medium-temperature ranges [16]. Whether the TEG modules are connected in series or parallel does not affect the system's maximum power output. The direction and flow rate of the fluid used to transfer heat to the TEG module also play a crucial role in determining the maximum power output. Counterflow configuration typically exhibits a higher power output compared to co-current configurations. Optimized TEG systems have demonstrated power output increases of over 34.6% [17].

Previous research has demonstrated that optimizing the TEM and enhancing the overall efficiency of the TEG system can be achieved by carefully considering various structural elements within the system that influence power production. While numerous studies have established a direct correlation between increased temperature difference and heightened power output in TEG systems, the impact of operating identical temperature-differences with varying heating and cooling sources on power generation remains unexplored. In this study, aim to address this gap in knowledge. By maintaining a consistent identical temperature-difference across the TEG system, Evaluate the influence of using distinct heating and cooling sources on power output. To achieve this, we will divide the two experiment conditions, each utilizing different hot and cold water temperatures. This approach will allow us to systematically evaluate the impact of heating and cooling source variations on power generation, providing valuable insights into optimizing TEG system performance.

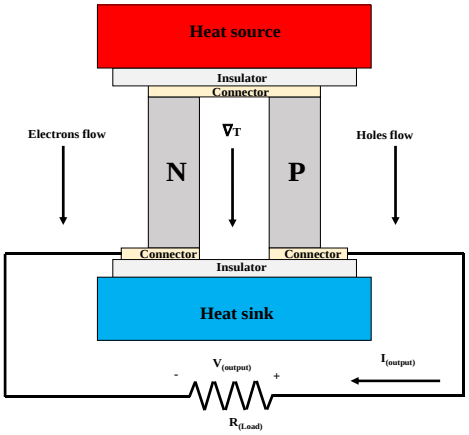

Fig. 1. Two-dimensional mechanism of thermoelectric generator.

2 Experimental design and method

In this work, it is an experiment to compare the results of the power output, by the TEG system using the identical temperature-difference two conditions, defined as the high temperature range (HTR) and the low temperature range (LTR). TEM in this experiment, consisting of Bismuth telluride N type and P type pellets total amount 142 elements, connected in an electrical series and thermally parallel, the module has an internal resistance of 2.8 ohms, The external resistance load used in this experiment is a Rheostat, which is adjusted the same maximum resistance of both conditions. To facilitate thermoelectric conversion, the TEM is strategically positioned to receive high temperatures on one side, designated as the hot side. A hot water source (HW) precisely regulates the temperature on the hot side of the HTR, maintaining it at $T_{(HW)}$ = 80 °C, while the LTR temperature is maintained at $T_{(HW)}$ = 65 °C. In contrast, the other side, referred to as the cold side, receives a low temperature. A cold water source (CW) meticulously controls the temperature on the cold side of the HTR, setting it to $T_{(CW)}$ = 20 °C, while the LTR temperature is maintained at $T_{(CW)}$ = 5 °C. The temperature differential between the two water sources is maintained at a constant 60 °C, denoted by $\Delta T_{(w)}$ = 60 °C, under both experimental conditions. The temperature of the water block is maintained at 25 °C. To ensure experimental consistency, the temperatures $T_{(HW)}$ and $T_{(CW)}$ must be precisely controlled and maintained at constant values. Subsequently, hot water and cold water are simultaneously introduced into the water block. Temperatures $T_{(HB)}$, $T_{(CB)}$, voltage output ($V_{(output)}$), and current output ($I_{(output)}$) are systematically recorded at 15-second intervals, denoted by $t_{(it)}$, as illustrated in Fig. 2 and Table 1. Upon reaching steady-state conditions, the measured values are calculated and expressed as follows. The temperature difference of the thermoelectric power generation system ($\Delta T_{(TEG)}$) and the generated power ($P_{(output)}$) are presented in Table 2 for both temperature range HTR and LTR conditions, under identical temperature-differences.

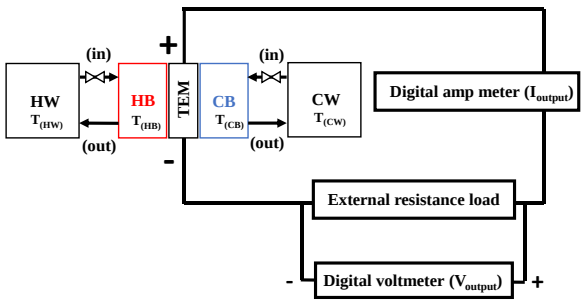

Fig. 2 . Schematic diagram of the thermoelectric power generator system experiment setup.

Table 1. Experimental setting of HW and CW water sources temperature and the interval time data record.

Temperature Condition	HTR	LTR
$T_{(HW)}$ (°C)	80	20
$T_{(CW)}$ (°C)	65	5
$\Delta T_{(W)}$ (°C)	60	
$t_{(it)}$ (sec)	15	

3 Result and discussion

To investigate the impact of varying temperature and electrical parameters over time, the experiment was conducted under two distinct conditions: HTR and LTR. Notably, both conditions maintained identical temperature-differences. Consider the temperature difference line $\Delta T_{(TEG)}$ at the water block position of both states. The lines overlap and converge at a steady state at 46 °C. Furthermore, the LTR condition exhibits a slightly faster transition to steady state compared to the HTR condition. This can be attributed to the smaller temperature difference between the LTR condition's HW position, and the initial temperature condition at the HB position compared to that of the HTR condition. This is illustrated in Fig. 3. The output power represents the primary outcome of operating the system under both experimental conditions. A comparison of the output power generated under both conditions reveals a significant difference. Despite maintaining identical temperature-difference as in the previous experiment, the LTR attains a steady state more rapidly than the HTR. Notably, operating the system under HTR conditions higher power output value compared to LTR, with a percentage difference of 5.85%, as illustrated in Fig. 4. The output power, the primary outcome of this electricity generation system, was determined from the output voltage across the load, reflecting the electric current flowing through the load. The results obtained under both conditions exhibit a consistent trend with the output power, with the HTR condition higher values compared to the LTR condition. As illustrated in Fig. 5 and 6, the percentage differences between the HTR and LTR conditions are 2.71% and 3.15%, respectively. A comprehensive summary of the experimental results is presented in Table 2. Output power is influenced by electrical resistance. The internal resistance varies with the temperature difference due to the fact that the TEM, the sole location receiving temperature in this system, operates continuously. This relationship between resistance and temperature difference is shown in [7]. A discernible influence of temperature on the electrical properties of thermoelectric materials is evident [8]. The observed disparity in electrical output suggests the presence of carrier mobility impediments within the TEM, which are responsible for the electric current in the TEG system. To theoretically explain these experimental findings, we must consider the impact of varying temperature on carrier mobility within thermoelectric materials. This relationship is governed

Table 2. Result of both conditions.

Temperature Condition	HTR	LTR
$T_{(HB)}$ (°C)	69	55
$T_{(CB)}$ (°C)	23	9
$\Delta T_{(TEG)}$ (°C)	46	
$V_{(output)}$ (V)	2.4554	2.3898
$I_{(output)}$ (A)	0.0742	0.0719
$P_{(output)}$ (W)	0.18219	0.17183
$V_{(\%diff)}$ (%)	2.71	
$I_{(\%diff)}$ (%)	3.15	
$P_{(\%diff)}$ (%)	5.85	

by two mechanisms, both of which highlight the connection between temperature and charge carrier mobility in thermoelectric materials. These mechanisms explain the observed differences in electrical power output between the HTR and LTR conditions, arising from the temperature gradient across the TEM. The fundamental principle governing thermoelectric materials is the mobility of charge carriers, a concept applicable to semiconductors. This mobility plays a critical role in understanding the behavior of thermoelectric materials. These materials are classified as extrinsic semiconductors, either n-type or p-type, with charge carriers, namely electrons and holes, serving as the driving force behind electricity generation. Within the TEG system, two mechanisms contribute to charge carrier scattering, impacting the mobility of charge carriers and ultimately influencing the system's electrical power output efficiency. Temperature fluctuations impact the internal structure of thermoelectric materials, consequently influencing the movement of charge carriers. When temperature variations lead to a reduction in the mean free time of carriers (τ) through both carrier scattering mechanisms, this directly affects the mobility of charge carriers (μ). This diminished mobility, in turn, reduces the current density within the system and the thermoelectric material (J), ultimately affecting the electric current (I) flowing through the system. This decreased mobility is attributed to the scattering of carriers within the thermoelectric material. This phenomenon has a direct bearing on the electrical conductivity of the material (σ), which also experiences a reduction. As a consequence, the power factor ($S^2\sigma$) within the ZT value also decreases, as per the relationship described in (2). This reduction in the power factor is a contributing factor to the diminished efficiency of the material for thermoelectricity generation. An analysis of the experimental data acquired at an identical temperature-difference of 46 °C demonstrates the existence of distinct carrier mobility conditions under both HTR and LTR conditions. This disparity stems from the differential temperature effects exerted on the hot and cold sides of the TEM under each condition. Two primary carrier scattering mechanisms governing these observations are lattice scattering and ionized impurity scattering, exhibiting temperature dependencies of $T^{(-3/2)}$ and $T^{(3/2)}$, respectively [18]. Furthermore, a well-established phenomenon in thermoelectric materials is

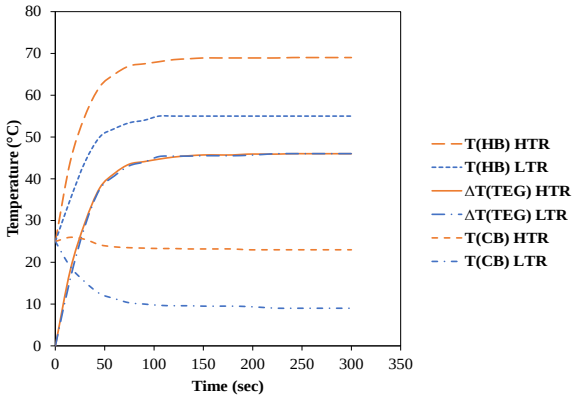

Fig. 3. Temperature results of HTR and LTR conditions with the identical temperature-difference at a steady state.

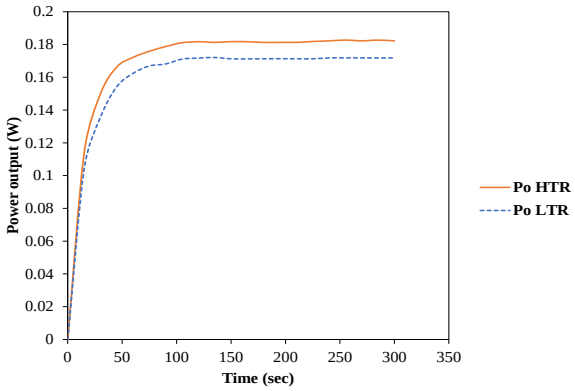

Fig. 4. Electric power output of HTR and LTR conditions with the identical temperature-difference at a steady state.

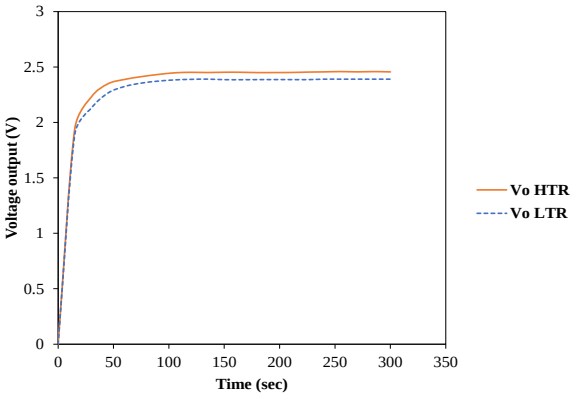

Fig. 5. Electric voltage output of HTR and LTR conditions with the identical temperature-difference at a steady state.

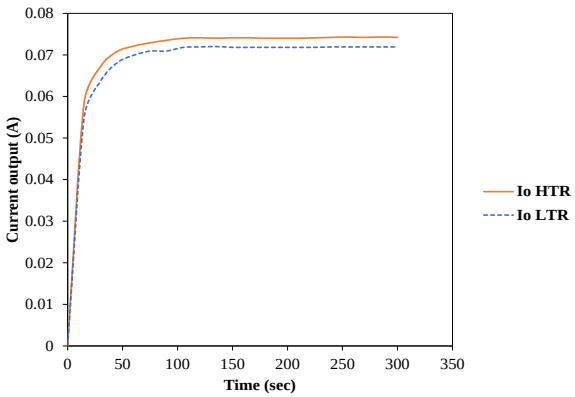

Fig. 6. Electric current output of HTR and LTR conditions with the identical temperature-difference at a steady state.

the reduction in carrier mobility with increasing temperature [8, 27]. In the context of n-type thermoelectric materials, corresponding p-type in this system experiences a temperature differential at the hot end, with 69 °C under HTR conditions and 55 °C under LTR conditions. The both temperature induces lattice scattering, despite the electron's thermal velocity and drift velocity being primarily driven by heat energy. As lattice vibrations intensify, electron mobility diminishes, leading to a reduction in the mean free time of electrons. However, under HTR conditions, the elevated temperature at the hot end serves as a driving force for carriers. As the electron current transported, the region where the temperature begins to decrease, inside n-type thermoelectric material, the carrier also possesses a thermal velocity, resulting in a higher residual kinetic energy compared to the LTR condition carriers as they approach the cold end. The cold end of the HTR and LTR conditions have temperatures of 23 °C and 9 °C, respectively. These two cold-end temperatures are significantly different, resulting in different scattering mechanisms. In this experiment, the LTR condition has a stronger influence on scattering with ionized impurities due to its lower temperature. This causes the carriers to have a lower thermal velocity. As a result, the carriers are more likely to be deflected by the ionized impurities, which reduces their mobility. In addition, the hot end of the LTR condition has less driving force for the carriers due to its lower hot-end temperature. When the carriers reach the cold end, their thermal velocity is further reduced. Therefore, the HTR condition exhibits higher current transport compared to the LTR condition. This observation aligns with the theory of carrier scattering mechanisms in extrinsic semiconductors, which states that the internal resistance of a thermoelectric material is influenced by hot and cold temperatures. Introducing an obstacle to the mobility of charge carriers within the TEG system reveals that HTR possesses lower electrical resistance compared to LTR, resulting in enhanced electrical power generation, as demonstrated in Fig. 4, 5, and 6 from experiments conducted with identical temperature-differences. However, the nature of these different temperature gradients induces variations in carrier mobility within the material, impacting the electrical current generated by the TEG system in this experiment. However, thermoelectric materials possess an appropriate operating temperature range, governed by their inherent properties. Considering the applicability of the TEG system operating under the HTR condition in this experiment, it is particularly suitable for TEG systems that require frequent startups, such as those employed in cooking stoves [15], or biomass stoves [19-26]. This condition is also well-suited for tropical to warm countries, as the cold-side temperature is closer to room temperature. In contrast, the LTR condition is more appropriate for TEG systems operating in cold-weather countries. This stems from the fact that the cold-side temperature under the LTR condition is significantly lower. Finally, to reduce the carrier scattering in thermoelectric materials, it will help to increase the efficiency of electricity generation. As these references show, the effect of carrier scattering mechanism [28-32]. The carrier scuttering is important for considering the operating temperature range of the system, which is conducive to better energy production in TEG systems.

4 Conclusion

In the experiment, under identical temperature-difference of 46 °C, the HTR condition demonstrated superior power output compared to the LTR condition, exhibiting a 5.85% enhancement. This improvement is attributed to both voltage and current outputs, which differ by 2.71% and 3.15%, respectively. The HTR condition exhibits favorable performance for TEG systems that require frequent on-off cycles, however, LTR conditions have promotable performance in cold weather applications.

We would like to express our sincere gratitude to the Department of Energy Technology and Management, Faculty of Science, Energy and Environment, King Mongkut's University of Technology North Bangkok for providing invaluable knowledge and access to research facilities.

References

1. D. Ji, H. Cai, Z. Ye, D. Luo, G. Wu, and A. Romagnoli, Comparison between thermoelectric generator and organic Rankine cycle for low to medium temperature heat source: A Techno-economic analysis. Sustain. Energy Technol. Assessment. **55**,102914(2023). https://doi.org/10.1016/j.seta.2022.102914
2. H. Seo, J. E. Cha, J. Kim, I. Sah, and Y.-W. Kim, Design and Performance Analysis of a Supercritical Carbon Dioxide Heat Exchanger. Appl. Sci. **10**, 4545 (2020). https://doi.org/10.3390/app10134545
3. P. Fernández-Yáñez, V. Romero, O. Armas, and G. Cerretti, Thermal management of thermoelectric generators for waste energy recovery. j.applthermaleng. **196**, 117291(2021). https://doi.org/10.1016/j.applthermaleng.2021.117291
4. E. Velmre, Thomas Johann Seebeck and his contribution to the modern science and technology, in 2010 12th Biennial Baltic Electronics Conference,IEEE,**17-24**(2010). https://doi.org/10.1109/BEC.2010.5631216
5. L. R. Kramer, A. L. O. Maran, S. S. de Souza, and O. H. Ando Junior, Analytical and Numerical Study for the Determination of a Thermoelectric Generator's Internal Resistance. Energ. **12**, 3053 (2019). https://doi.org/10.3390/en12163053
6. Z. Wu et al., Heat and electric flux coupling of closed-loop thermoelectric generator. Energy Convers. Manage. **244**, 114529 (2021). http://doi.org/10.1016/j.enconman.2021.114529
7. O. Ando Junior, N. Calderon, and S. de Souza, Characterization of a Thermoelectric Generator (TEG) System for Waste Heat Recovery. Energ. **11**,1555(2018). https://doi.org/10.3390/en11061555

8. I. T. Witting et al., The Thermoelectric Properties of Bismuth Telluride. Adv. Electron. Mater. 5, (2019). https://doi.org/10.1002/aelm.201800904
9. S. Lv, M. Liu, W. He, X. Li, W. Gong, and S. Shen, Study of thermal insulation materials influence on the performance of thermoelectric generators by creating a significant effective temperature difference. Energy Convers. Manage. **207**, (2020). https://doi.org/10.1016/j.enconman.2020.112516
10. H.-J. You, H.-S. Chu, W.-J. Li, and W.-L. Lee, Influence of different substrate materials on thermoelectric module with bulk legs. J. Power Sources. **438**, 227055 (2019). https://doi.org/10.1016/j.jpowsour.2019.227055
11. O. I. Ibeagwu, Modelling and comprehensive analysis of TEGs with diverse variable leg geometry. Energ. **180**, 90-106 (2019). https://doi.org/10.1016/j.energy.2019.05.088
12. X. Wang et al., Enhanced thermoelectric figure of merit in nanostructured n-type silicon germanium bulk alloy. Appl. Phys. Lett. **93**, 193121 (2008). https://doi.org/10.1063/1.3027060
13. G. Joshi et al., Enhanced thermoelectric figure-of-merit in nanostructured p-type silicon germanium bulk alloys. Nano Lett. **8**, 4670-4674 (2008). https://doi.org/10.1021/nl8026795
14. N. Jaziri, A. Boughamoura, J. Müller, B. Mezghani, F. Tounsi, and M. Ismail, A comprehensive review of Thermoelectric Generators: Technologies and common applications. j.egyr. **6**, 264-287 (2020). https://doi.org/10.1016/j.egyr.2019.12.011
15. D. Champier, J. P. Bedecarrats, M. Rivaletto, and F. Strub, Thermoelectric power generation from biomass cook stoves. Energ. **35**, 935-942 (2010). https://doi.org/10.1016/j.energy.2009.07.015
16. T. Sakamoto et al., Selection and Evaluation of Thermal Interface Materials for Reduction of the Thermal Contact Resistance of Thermoelectric Generators. J. Electron. Mater. **43**, 3792-3800 (2014). http://doi.org/10.1007/s11664-014-3165-7
17. J. Chen et al., Enhanced Efficiency of Thermoelectric Generator by Optimizing Mechanical and Electrical Structures. Energ. **10**,1329 (2017). https://doi.org/10.3390/en10091329
18. S. M. Sze, Y. Li, and K. K. Ng, Physics of semiconductor devices. John wiley & sons, (2021).
19. K. Sornek, M. Filipowicz, and K. Rzepka, The development of a thermoelectric power generator dedicated to stove-fireplaces with heat accumulation systems. Energy Convers. Manage. **125**, 185-193 (2016). https://doi.org/10.1016/j.enconman.2016.05.091
20. G. F. Rinalde, L. E. Juanicó, E. Taglialavore, S. Gortari, and M. G. Molina, Development of thermoelectric generators for electrification of isolated rural homes. Int. J. Hydrogen Energy. **35**, 5818-5822 (2010). https://doi.org/10.1016/j.ijhydene.2010.02.093
21. A. Montecucco, J. Siviter, and A. R. Knox, Combined heat and power system for stoves with thermoelectric generators. Appl. Energy. **185**, 1336-1342 (2017). https://doi.org/10.1016/j.apenergy.2015.10.132
22. A. Montecucco, J. Siviter, and A. R. Knox, A Combined Heat and Power System for Solid-fuel Stoves Using Thermoelectric Generators. Energy Procedia. **75**, 597-602 (2015). https://doi.org/10.1016/j.egypro.2015.07.462
23. G.-n. Li, S. Zhang, Y.-q. Zheng, L.-y. Zhu, and W.-w. Guo, Experimental study on a stove-powered thermoelectric generator (STEG) with self starting fan cooling. j.renene. **121**, 502-512 (2018). https://doi.org/10.1016/j.renene.2018.01.075
24. G. Li, Y. Zheng, J. Hu, and W. Guo, Experiments and a simplified theoretical model for a water-cooled, stove-powered thermoelectric generator. Energ. **185**, 437-448 (2019). https://doi.org/10.1016/j.energy.2019.07.023
25. D. Champier, J. P. Bédécarrats, T. Kousksou, M. Rivaletto, F. Strub, and P. Pignolet, Study of a TE (thermoelectric) generator incorporated in a multifunction wood stove. Energ. **36**, 1518-1526, (2011). https://doi.org/10.1016/j.energy.2011.01.012
26. M. Araiz, Á. Casi, L. Catalán, Á. Martínez, and D. Astrain, Prospects of waste-heat recovery from a real industry using thermoelectric generators: Economic and power output analysis. Energy Convers. Manage. **205**, 112376 (2020). https://doi.org/10.1016/j.enconman.2019.112376
27. T. Witting, F. Ricci, T. Chasapis, G. Hautier, G. J. Snyder, unpublished.
28. K. Wu, L. Huang, C. Y. Wu, and G. Yu, Effects of scattering mechanisms on thermoelectric properties of bismuth. Solid State Commun. **390**, 115471 (2024). https://doi.org/10.1016/j.ssc.2024.115471
29. R. P. Chasmar and R. Stratton, The Thermoelectric Figure of Merit and its Relation to Thermoelectric Generators. Journal of electronics and control. **7**, 52-72 (2007). https://doi.org/10.1080/00207215908937186
30. Y. Qin, Y. Xiao and L. D. Zhao, Carrier mobility does matter for enhancing thermoelectric performance. APL Mater. **8**, 010901 (2020). https://doi.org/10.1063/1.5144097
31. Md. G. Rosul, M. Zebarjadi, Effect of Electron-Phonon Interaction and Ionized Impurity Scattering on the Room Temperature Thermoelectric Properties of Bulk MoSe2. J. Phys. Chem. C. **126**, 15011–15018 (2022). https://doi.org/10.1021/acs.jpcc.2c03782
32. L. Pan, S. Mitra, L. Zhao, Y. Shen, Y. Wang, C. Felser and D. Berardan, The Role of Ionized Impurity Scattering on the Thermoelectric Performances of Rock Salt $AgPb_mSnSe_{2+m}$. Adv. Funct. Mater. **26**, 5149-5157 (2016). https://doi.org/10.1002/adfm.201600623